A Virtual Mechanical Interaction Layer Enables Resilient Human-to-Robot Object Handovers

Omar Faris¹, Sławomir Tadeja², and Fulvio Forni¹

Abstract—Object handover is a common form of interaction that is widely present in collaborative tasks. However, achieving it efficiently remains a challenge. We address the problem of ensuring resilient robotic actions that can adapt to complex changes in object pose during human-to-robot object handovers. We propose the use of Virtual Model Control to create an interaction layer that controls the robot and adapts to the dynamic changes in the handover process. Additionally, we propose the use of augmented reality to facilitate bidirectional communication between humans and robots during handovers. We assess the performance of our controller in a set of experiments that demonstrate its resilience to various sources of uncertainties, including complex changes to the object's pose during the handover. Finally, we performed a user study with 16 participants to understand human preferences for different robot control profiles and augmented reality visuals in object handovers. Our results showed a general preference for the proposed approach and revealed insights that can guide further development in adapting the interaction with the user.

I. Introduction

Human-to-robot object handover is a fundamental task that frequently occurs in collaborative manipulation. Safe and efficient human-to-robot object handover represents a key requirement for broader human-robot collaboration [1]. However, compared to the smooth and seamless interactions between humans, achieving that same level of safety and efficiency with robots remains a significant challenge [2].

Prior research have focused on recognizing and communicating human and robot intentions [3]–[5], detecting and grasping objects with diverse physical properties [6]–[8], and ensuring safety throughout the process [9], [10]. In particular, a central issue seems to be the ability to understand and react to the continuous changes that occur during the handover process [2]. This is the robot's ability to effectively adapt and respond to various factors that can influence the handover task, particularly the variability and unpredictability of human motion. We summarize this with the concept of *resilient* handover, in contrast to non-resilient cases that force the human to maintain a static giving pose or adhere to a fixed handover location, thereby imposing unnatural constraints and uncomfortable strain.

Various approaches to developing such resilient and reactive robotic actions in human-to-robot object handovers have been studied, including handling different human hand poses [11], responding to changes in the object pose [12], [13], reacting to sudden human hand motion [14], avoiding hand collision and occlusion [15], tracking the object

through visual servoing [16], predicting handover locations [17], and learning generalizable grasps from simulations and demonstrations [18]. However, these approaches generally focus on producing resilient robotic behaviors by addressing limitations closely associated with robot grasping, e.g., predicting future grasp poses [13] or continuously monitoring and updating the selected grasp [12]. In contrast, our work examines this problem from the perspective of *motor coordination* between the robot and the human, who together form a coordinated ensemble regulated by an interaction layer. Given a grasping pose for a specific human-to-robot object handover, the aim is to create resilient human-robot interactions by ensuring a smooth, responsive, reactive, and safe coordination between robot and human.

Human-to-robot object handovers are complex because the robot and the human continuously influence each other. Each handover is different from the previous one, and uncertainties dominate the whole process (interaction dynamics, incomplete sensing, human decisions, etc.). Our hypothesis is that this complexity can be mitigated by introducing an interaction layer for coordination that works as a low-level controller, shaping the feedback loop between the human and the robot to safely adapt the robot behavior without compromising speed and performance. The functional modules composing this interaction layer are illustrated in Fig. 1.

Our proposed interaction layer takes the form of a 'virtual' mechanism, following the philosophy of Virtual Model Control [19], [20]. Virtual model control has demonstrated promising results in diverse tasks ranging from locomotion of bipedal [21] and quadruped robots [22], [23], to reaching tasks while avoiding obstacles [24], and robotic surgery [20], [25]. In this work, we utilize virtual links, joints, springs, and dampers, to shape the desired robotic reactions. Through hand-pose estimation, the terminals of our virtual interconnection mechanisms are attached to the robot and to the human hand. This configuration generates virtual forces that drive the robot motion. The coordination and motion of the robot are the direct result of this 'mechanical' interaction between robot and human, mediated by the virtual components.

We make use of augmented reality as a key technical enabler for our implementation, which has shown promising results for human-robot bidirectional communication in various scenarios [26], [27]. In this work, a head-mounted display tracks the user's hand and shares that information with the robot while also visualizing the intended grasping pose of the robot, which is adapted continuously to reflect the real-time adjustments of the robot motion towards the

¹Department of Engineering, University of Cambridge, UK.

²Department of Mechanical Engineering, Massachusetts Institute of Technology

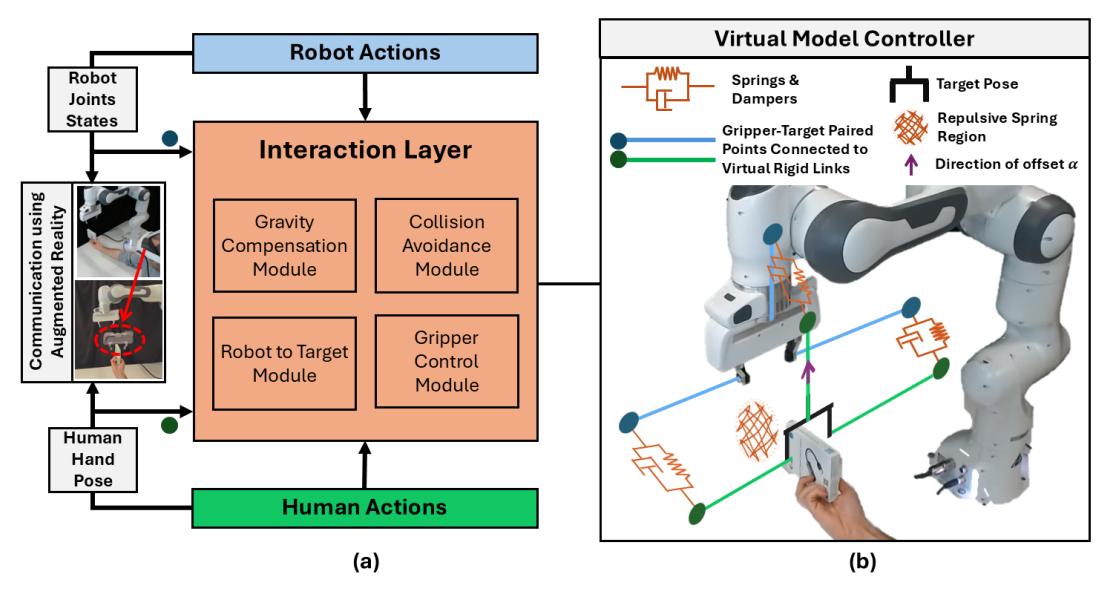


Fig. 1: (a) Human-to-robot object handover is shaped by continuous human-robot interactions, coordinated through the Interaction Layer. An Augmented Reality device enables human-robot bidirectional communication by sensing the human hand pose and receiving the robot joints states to visualize the robot intent to the human user. (b) Our Virtual Model Control implementation of the interaction layer. The Main Controller Module consists of Gripper-Target Paired Points (target points are translated by an offset α) connected to the gripper and the object/hand through Virtual Rigid Links, with Springs and Dampers between each pair. Repulsive Spring Regions form the Auxiliary Controller Module, where one region is placed here in front of the hand and the object. In this implementation, the Gripper Control Module is not controlled by the Virtual Model Controller due to hardware limitations.

object. This visualization allows the user to understand what the robot is thinking, potentially acting accordingly, and has previously demonstrated better human-to-robot object handovers [28].

To evaluate our approach, we completed a series of experiments that assess the resilience of the virtual model control interaction layer against various perturbations during human-to-robot object handovers. We have also conducted a human user study to validate the usability of our solution with different users and investigate the effectiveness of utilizing augmented reality as a bidirectional communication medium.

II. RESILIENT HUMAN-ROBOT INTERACTION LAYER

A. Proposed Virtual Model Controller

We have identified two major factors for enabling resilient human-robot interactions:

- While reaching objects within its workspace, the robot should seamlessly and continuously adapt to position and orientation changes of the object, as long as this is in the hands of the human.
- In approaching the object, the robot should be be able to negotiate a collision-free path, avoiding both the human and the object.

We construct a virtual model controller consisting of two modules to realize these features. The Main Controller Module generates virtual attraction forces that drive the robot towards the object, enabling responsive robot actions when the object is moved. In contrast, the Auxiliary Controller Module generates region-specific repulsive forces to guarantee collision avoidance. These modules do not require the solution of inverse kinematics or the completion of any motion planning computation. The robot's intelligent and reactive behavior is determined by the set of virtual springs, dampers, and linkages defined within the virtual model control framework, effectively reducing complex control to fundamental virtual mechanical interactions.

1) Main Controller Module: For a two-fingered gripper, this module is represented by three virtual massless pairs of points. Each pair consists of a gripper point rigidly connected to the robot's gripper (blue points in Fig. 1b), a target point connected to the object or the hand (green points in Fig. 1b), and virtual attractive springs and dampers between them. By using multiple connection points we can control the pose of a two-fingered gripper while keeping its fingers at the appropriate grasping target.

In this paper, the target points are rigidly connected to the object. Any changes in the object pose extend or shrink the lengths of virtual springs and dampers, forcing the gripper to move accordingly, typically towards the object. The geometry of these connection points is regulated by the virtual rigid links represented in Fig. 1b. These extend from gripper and object, with the virtual connection points placed at the end of them. Increasing the length of these links results in higher forces when the object is rotated, enabling the gripper to swiftly respond to the object motion with the right orientation.

Saturated spring force profiles of the form

$$\mathbf{F}_{s} = F_{s_{max}} \tanh\left(\frac{k_{s}|\mathbf{p}|}{F_{s_{max}}}\right) \frac{\mathbf{p}}{|\mathbf{p}|} \tag{1}$$

are used to generate forces between gripper-target paired points. This prevents the robot from applying excessive forces for large spring extension. In (1), $F_{s_{max}}>0$ is the maximum force that a spring can apply, $k_s>0$ is the spring's stiffness, and $\mathbf{p}\in\mathbb{R}^3$ is the displacement vector between paired gripper-target points.

The elastic force generated at each pair of gripper-target points is regulated by two saturated springs. The first has a large maximal force $F_{s_{max_1}}$ but low stiffness k_{s_1} while the second relies on a low maximal force $F_{s_{max_2}}$ but high stiffness k_{s_2} . The first spring governs large-distance interactions but has limited effects locally. The second spring has limited long-distance interaction but provides a snap-like mechanism at close range. This is illustrated in Fig. 2a.

Virtual dampers generate forces of the form

$$\mathbf{F}_d = c(|\mathbf{p}|)\dot{\mathbf{p}},\tag{2}$$

characterized by the position dependent damping c(s)>0 for all $s\geq 0$. As before, ${\bf p}$ refers to the displacement vector between a generic pair of gripper-target points. In particular, we use

$$c(|\mathbf{p}|) = c_1 + c_2 \tanh(\beta|\mathbf{p}|) \tag{3}$$

where $c_1 \geq 0$ is a constant representing the minimum damping coefficient, $c_1+c_2\geq 0$ is the maximal damping coefficient, and β shapes the sensitivity of the damping coefficient to variations in position. Variable damping gives us further tuning flexibility and has proven effective in experiments.

An offset α ($\alpha=10$ cm, determined experimentally) is introduced to the position of the target points, to keep a safe distance between the gripper fingers and the object. The offset translates the target points in the direction of the gripper base (see the arrow in Fig. 1b). Reducing this offset brings the gripper closer to the object. This is done in the last phase of grasping (as detailed in Section II-C).

2) Auxiliary Controller Module: This module implements collision avoidance by realizing a virtual repulsive region around the human hand and the object. In combination with the Main Controller Module, the robot can negotiate a collision-free path while reaching the target. The repulsive action is defined by several spherical repulsive regions, each implemented by a repulsive spring with a Gaussian-like force magnitude profile. Given the energy $E = k_r \sigma_r^2 e^{\left(\frac{-|\mathbf{p}|^2}{2\sigma_r^2}\right)}$,

$$\mathbf{F}_r = -|\mathbf{p}_r|k_r e^{(\frac{-|\mathbf{p}|^2}{2\sigma_r^2})} \tag{4}$$

where $k_r > 0$ is the stiffness, σ_r is the distance at which the repulsive region applies its maximum repulsion force, and \mathbf{p}_r is the displacement vector between the center of the repulsive region and the gripper fingers. If we define $k_r = \frac{F_{r_{max}}}{\sigma_r} e^{0.5}$, then the parameter $F_{r_{max}}$ represents the maximum force the repulsive spring can applies. In particular, the maximum force $F_{r_{max}}$ is generated at the distance $|\mathbf{p}_r| = \sigma_r$.

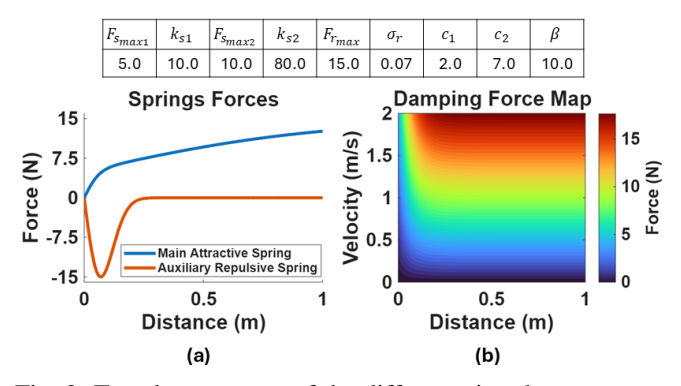


Fig. 2: Tuned parameters of the different virtual components used in our virtual model control along with their force profiles: (a) main and auxiliary springs and (b) main dampers. Units are N for force values, N/m for stiffness coefficients, N s/m for damping coefficients, and m for σ_r .

The number and placement of these regions depend on the task. For simplicity, in our experiments we only protect the space in front of the object/hand, using a single single spherical repulsive region with its center always at a distance β ($\beta=23$ cm, determined experimentally) from the hand, as shown in Fig. 1b.

B. Virtual Model Controller Implementation

In virtual model control [19], [20], each component of the virtual mechanisms (i.e., springs and dampers) applies a force \mathbf{F}_i at a point \mathbf{p}_i on the robot body to realize the desired behavior. For a robot arm whose revolute joints have coordinates \mathbf{q} , the point \mathbf{p}_i can be expressed as a function of the joint coordinates $\mathbf{p}_i = \mathbf{h}_{\mathbf{p}_i}(\mathbf{q})$, and the forces from all the virtual components are translated into joint torques $\boldsymbol{\tau}$ by

$$\tau = \sum_{i=1}^{n} \mathbf{J}_{\mathbf{p}_{i}}^{T}(\mathbf{q}) \mathbf{F}_{i}, \tag{5}$$

where $\mathbf{J}_{\mathbf{p}_i}^T(\mathbf{q})$ is the transpose of the Jacobian matrix $\mathbf{J}_{\mathbf{p}_i}(\mathbf{q}) = \frac{\partial \mathbf{h}_{\mathbf{p}_i}(\mathbf{q})}{\partial \mathbf{q}}$. We refer the reader to [20] for a detailed characterization of virtual model control.

We use the software package VMRobotControl.jl package [29] for implementing the controller on a Franka Emika Panda robot arm equipped with the Franka Hand gripper. The package simplifies the design of virtual model control mechanisms and components and facilitate their integration with robot manipulators. Furthermore, it provides a simulation environment that facilitates the evaluation of the virtual mechanism behavior and its interaction with the robot, as well as rapid iteration of controller parameters. We utilize the VMRobotControl.jl simulation environment to design and tune the proposed virtual model controller, followed by fine-tuning on the real robot through trial and error. The length of the rigid links attached to gripper and object was set at 45 cm upon experimentally observing the robot's reaction to rotating and moving the hand. Larger lengths led to instability and response issues, such as gripper oscillations following small hand rotations (due to the finite



Fig. 3: Objects used in the experiments and their grasping pose as seen through the augmented reality interface: (left to right) a cardboard box, a banana, a spoon, and a plastic cup.

bandwidth of the joint actuators). Shorter lengths made the robot less reactive. All remaining parameters (stiffness and damping) are summarized in Fig. 2.

C. Gripper Control Module

The final grasping and handover action is handled by a standalone module to mitigate the lack of torque/force control ability of the hardware adopted in our experiment (Franka Hand gripper). When the Gripper Control Module is activated, the gripper moves closer to the object by reducing the offset α to zero, followed by a closure of the gripper fingers to complete the task. To activate this module, two conditions must be satisfied: (i) the hand velocity is low and (ii) all the distances between paired gripper-target points must be below a certain value d, set experimentally at 10 cm. Grasping is then initiated after at least one second if all these distances are < 5 cm.

This module runs in parallel with the the interaction layer. Therefore, if the hand moves when the grasping action is not complete, the module is deactivated by resetting the controller offset α to 10 cm and reopening the gripper. Hence, the handover process is not interrupted until the grasping action is complete.

III. BIDIRECTIONAL COMMUNICATION USING AUGMENTED REALITY

We utilize augmented reality to facilitate human-robot bidirectional communication, given its potential to enhance human-robot interaction [26], [30]. We rely on the Meta Quest 3 headset to harness its hand-tracking capability and leverage it as a communication medium. From the Quest 3, the robot receives the measured hand palm pose, whereas the human sees a visualization of the expected grasping pose. This enables the human to modify the hand pose and therefore the object pose before the robot attempts to grasp it, thereby improving the likelihood of successful handover.

We use the Meta XR All-in-One SDK and the Unity game engine for programming the Quest 3 and communicating with the robot. From the SDK, the Mixed Reality Utility Kit (MRUK) API is used to scan the room and calibrate the robot location in the Quest 3 coordinate frame. The latter is only performed once by placing a MRUKAnchor on the robot origin. Then, the MRUK tool loads the room scanning, including detection of any MRUKAnchor in the room, whenever the device is launched in the saved area.

As the Quest 3 does not provide access for object detection and tracking, we generate the positions of the controller target points by inferring information from the tracked human hand pose detection and known object shapes (see Fig. 3). The hand-tracking is available directly in Quest 3, represented as a hand skeleton with 26 points. In this work, we only consider the pose of the hand palm and use a low-pass filter to process the raw pose readings from the Quest 3, as well as a Kalman filter to estimate the hand velocity, which is subsequently used in the Gripper Control Module.

IV. RESILIENT HUMAN-TO-ROBOT OBJECT HANDOVERS

A. Experimental Protocol

We evaluated our controller in two experiments that cover a significant set of realistic scenarios. Experiment I considers handover with different objects that are also moved by the user (translation and/or rotation) after the robot starts to reach them. This experiment evaluates the robot's resilience to changes in the expected grasping pose due to variable sizes and shapes of the objects and object movements, such that the robot can continue the handover process in the presence of unpredictable human hand motion. Experiment II looks into randomized robot starting poses and also extends the set of potential object movements to include complex sequences of movements at different times. These experiments are supplemented with a user study to evaluate the user experience in interacting with the robot, alongside the AR's feasibility for communication.

In each experimental run, a person holds an object in the hand in a fixed predetermined position compatible with the grasping capability of a two-finger gripper (see Fig. 3 for an example). The robot's external enabling device is pressed to initiate the robot's movement. Each experimental run ends when the robot gripper closes its fingers on the object as we do not consider the post-handover phase. The handover is considered successful if the object is grasped successfully. When counting the failures, we discard any attempt that failed for reasons unrelated to the task. This excludes from the analysis failures due to communication loss in the system and to issues with the hand-tracking algorithm of the Meta Quest 3.

TABLE I: Performance metrics. The figure shows the points used to calculate the distance-related metrics.

Metric	Definition					
	Approach time from when the robot starts					
t_a	moving till the gripper closes on the object					
SR	Success rate of the object handover					
d_i	Initial distance between the robot and the object					
L_r	Total path length covered by the robot motion					
L_o	Total path length covered by the object motion					
	Distance error between the gripper points					
e_d	and the target points during the grasping					
θ_i	Initial angle difference between					
σ_i	the robot and the initial expected pose					
θ_r	Difference of the robot angle					
σ_r	between the start and end of experiment					
θ_{o}	Difference of the object angle					
00	between the start and end of experiment					
60	Error in angle between the gripper points					
e_{θ}	and the target points during the grasping					



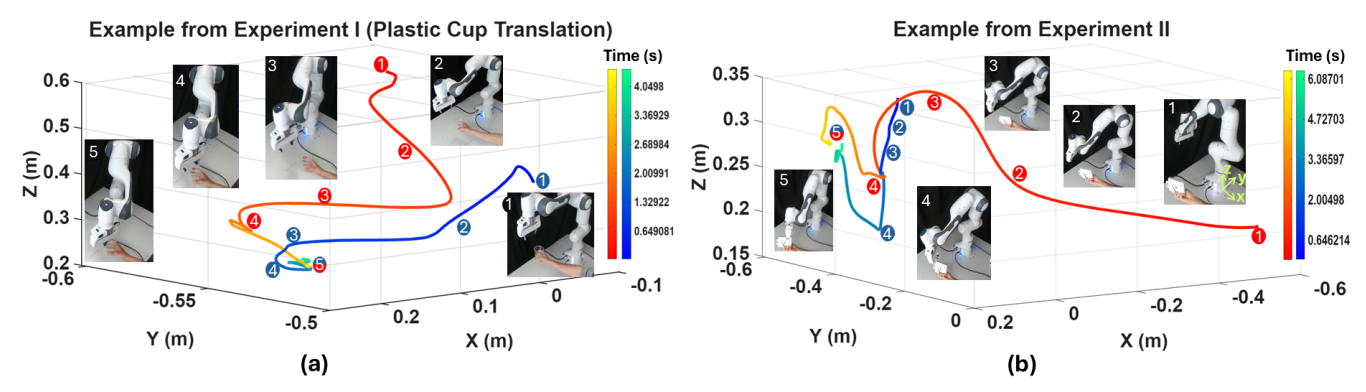


Fig. 4: Examples of trajectories from the gripper right finger (red) and its corresponding target point (blue) with temporal markers of recorded snapshots, where (a) is a plastic cup translation example from Experiment I with the object being moved after the robot starts moving and (b) is an example from Experiment II highlighting the effect of the Auxiliary Controller Module with a spherical repulsive region in front of the object pushing the gripper above the object between markers 2 and 3 (instead of continuing through a straight line). Robot coordinate system used as the reference frame is shown in photo 1 of (b). Full experimental runs of the presented trajectories are shown in the Supplementary Video.

TABLE II: Mean (standard deviation) of the proposed metrics for Experiment I

		1.5						
	Cardboard Box		Banana		Spoon		Plastic Cup	
	Rotation	Translation	Rotation	Translation	Rotation	Translation	Rotation	Translation
$\overline{t_a}$	3.38 (0.34)	4.79 (0.54)	3.14 (0.37)	4.14 (0.58)	3.64 (0.91)	4.30 (0.39)	3.80 (0.52)	4.76 (0.86)
SR	100%	100%	100%	100%	95%	100%	100%	100%
$\overline{d_i}$	30.88 (3.42)	22.67 (4.51)	26.63 (2.47)	19.76 (2.79)	27.05 (2.63)	25.15 (4.46)	33.69 (3.46)	26.90 (7.62)
L_r	47.43 (4.70)	68.55 (14.32)	49.44 (4.37)	63.97 (12.26)	46.66 (5.81)	66.21 (11.30)	50.22 (6.59)	73.62 (19.52)
L_o	15.97 (4.14)	52.84 (18.68)	20.88 (4.09)	42.56 (12.67)	19.99 (3.46)	39.27 (12.33)	20.49 (6.70)	53.43 (19.45)
e_d	2.02 (1.02)	1.79 (0.44)	3.88 (0.47)	3.06 (0.78)	3.44 (1.21)	3.42 (0.88)	2.63 (0.74)	1.95 (0.71)
$\overline{\theta_i}$	16.54 (3.78)	11.86 (4.68)	94.27 (6.13)	98.77 (4.17)	86.41 (13.61)	83.57 (4.41)	12.62 (5.62)	13.01 (4.28)
$\overline{\theta_r}$	38.43 (7.02)	20.87 (5.90)	107.73 (7.02)	97.73 (5.25)	103.98 (18.49)	90.16 (6.80)	43.85 (10.89)	14.89 (4.28)
$\overline{\theta_o}$	30.88 (6.45)	12.70 (5.49)	43.29 (10.99)	16.36 (8.07)	52.20 (24.41)	13.99 (5.48)	40.44 (11.71)	9.86 (3.68)
e_{θ}	2.46 (1.07)	2.51 (1.33)	3.69 (1.81)	3.04 (1.26)	3.46 (2.13)	5.05 (1.57)	1.97 (0.88)	1.96 (0.82)

TABLE III: Mean (standard deviation) of the metrics for Experiment II

t_a	SR	d_i	L_r	L_o	e_d	θ_i	θ_r	θ_o	e_{θ}
6.79 (0.91)	100%	61.89 (8.16)	122.31 (16.79)	55.50 (18.07)	2.32 (0.75)	69.19 (30.27)	78.52 (29.99)	31.55 (15.24)	2.97 (1.46)

B. Experimental Metrics

We acquire a comprehensive set of metrics to evaluate the handover process performance, summarized in Table I. Each experimental run begins when the external activation device is pressed (i.e., the robot starts moving) and ends when the gripper fingers close.

Distance-related metrics (d_i, L_r, L_o, e_d) are all calculated from the points illustrated in Table I. Yellow-red point pairs are used for d_i and e_d . Red points are used for L_o , whereas yellow points are used for L_r . The largest of the three values is reported in the results. Angles are calculated based on the axis-angle representation formed by the relative rotation matrix between the two relevant rotation matrices. For example, in the case of θ_r , the two rotation matrices are formed by the three virtual model control points attached to the robot at its initial pose and at its final pose.

The approach time is correlated to the distance or angle traveled by the robot, which influences the duration of a given experiment. If the object moves a short distance, the experiment will be naturally shorter and vice-versa.

Likewise, the path length covered by the robot is correlated to the movement of the object and to the initial distance and angle between the robot and the object.

The errors in distance and angle between the target points and the gripper points provide insights into the controller's performance under current settings, and its suitability for other objects (e.g., a tiny object may require stronger spring stiffness to reduce errors, which may negatively affect other aspects of the system).

C. Experiment I: Object Translation and Rotation

In this experiment, four objects requiring different grasping poses are moved randomly, either by translation or rotation, immediately after the robot starts moving. The robot always starts from the same initial pose. This allows us to build a comparison with existing human-to-robot object handover pipelines with a similar experimental protocol [12], [13], [15]. We perform 20 randomized experimental runs for each object (shown in Fig. 3) and each type of motion (either rotation or translation).

Our proposed controller achieves high success rates across

all tests, as summarized in Table II. The mean approach time was less than 4s when the object was rotated and less than 5s for translations. This demonstrates the proposed interaction layer's ability to quickly adapt and handle the tested pose changes. The final distance and angle errors varied among objects, likely caused by poses that are intrinsically more difficult and less reachable given the robot kinematics. This is the case of both banana and spoon grasping (large initial angle θ_i in addition to the induced motion). Compared to other works [12], [13], [15], our method exhibits a faster approach time and a slightly better success rate when compared to similar objects and tests (see Table I in [12], [13] and Fig. 4 in [15]).

Fig. 4a provides an illustration of the trajectories of the gripper right finger and its paired target point associated to a plastic cup. This is a translation experimental run, with markers 1 to 5 corresponding to snapshots from the recorded video. Starting at marker 1, the object was moved away from the robot, which resulted in the extension of the virtual springs and dampers causing the robot to closely follow the target point. At marker 4, the hand was nearly static and there was close proximity between the object and the gripper. This activated the Gripper Control Module. The robot executed a final approach until grasping was achieved, at marker 5.

D. Experiment II: Random Starting Pose and Movements

In this experiment, we complete 20 runs randomizing the robot starting pose and object trajectory. The object is moved after activating the Gripper Control Module. This experiment demonstrates the robot's ability to reach the object regardless of its starting pose. We also show how the robot handles scenarios where the object is moved after triggering the final approach of the Gripper Control Module. For simplicity, we limit this experiment to the cardboard box object.

Successful robot grasping is consistently achieved in all experimental runs. In comparison to the previous experiment, both e_d and e_θ were higher, albeit without a strong effect on the success rate (see Table III). When the gripper starting pose was below the human hand, the Auxiliary Controller Module enabled the robot to conveniently approach the object from the top, as shown in Fig. 4b. The robot was pushed upwards between markers 2 and 3. This prevented a potential collision with the object. At marker 4, the object was pulled away by the user right after the Gripper Control Module triggered an attempt to grasp. The reactive behavior granted by the interaction layer allowed the robot to move towards the new position of the object, achieving a successful grasping at marker 5.

E. Further considerations and limitations

The results strongly support our hypothesis that a humanrobot interaction layer based on virtual model control enables resilient human-to-robot object handovers. Nonetheless, there are certain cases where the current method may not offer an effective solution. With the proposed virtual model controller, the robot struggles to continue the handover efficiently when some of its joints are close to their limits. A similar problem is observed when the object is too close to the robot body links. The impact of these cases can be mitigated through the design of additional virtual components. We also observe that the proposed virtual model control is designed for two-fingered grippers. Extensions to multi-fingered grippers appear to be straightforward, through the design of additional virtual rigid links and gripper-target pairs. However, because of the limits of our current setting, this remains untested.

V. USER STUDY

A. Experimental Conditions

We conducted a user study to evaluate the performance of our method across different users and to understand user preferences in augmented reality-based human-to-robot object handovers. Four conditions were considered with two different robot profiles and the presence and absence of augmented reality-based visuals. Condition A had the augmented reality visuals turned on and the same virtual model control parameters used in the previous experiments. resulting in an authoritative, highly resilient robot that can handle the handover by itself. Condition B had the same authoritative robot but without the augmented reality visuals. Condition C had augmented reality visuals turned on, but with a slower, less resilient robot that required the human to bring the object closer to the robot, resulting in a more cooperative nature of the handover. Finally, Condition D kept the slow, cooperative robot profile without the augmented reality visuals. The cooperative robot profile was enabled by setting $F_{s_{max_2}}$ to zero.

B. Participants and Experimental Protocol

We recruited 16 participants (8 females and 8 males) through opportunity sampling. They were between 23 and 34 years old ($M=28.06,\ SD=3.17$), and none of them had prior experience with augmented reality; however, 13 participants reported varying levels of earlier exposure to virtual reality. Moreover, 9 participants had experience with robotics, with 8 reporting extensive exposure, while the remaining 7 had no prior exposure to robotics.

We asked the participants to move an object in a single motion stroke after the robot started moving. For simplicity, participants were encouraged to perform a translation motion of the object. In Conditions A & B, participants were told to stop moving after that and wait for the robot to grasp the object, in contrast to Conditions C & D where they were asked to wait for the robot to approach them and move the object to it afterwards. The order of the conditions was randomized so that each participant performed a unique sequence of conditions.

Each participant was shown one demonstration of each condition, accompanied by a translation motion of the object, before starting the experiments. In addition, a five-minute familiarization phase was provided with Quest 3 to understand how the visuals work and align the object as necessary (without operating the robot). Each participant was asked to perform three experimental runs. When users did not follow

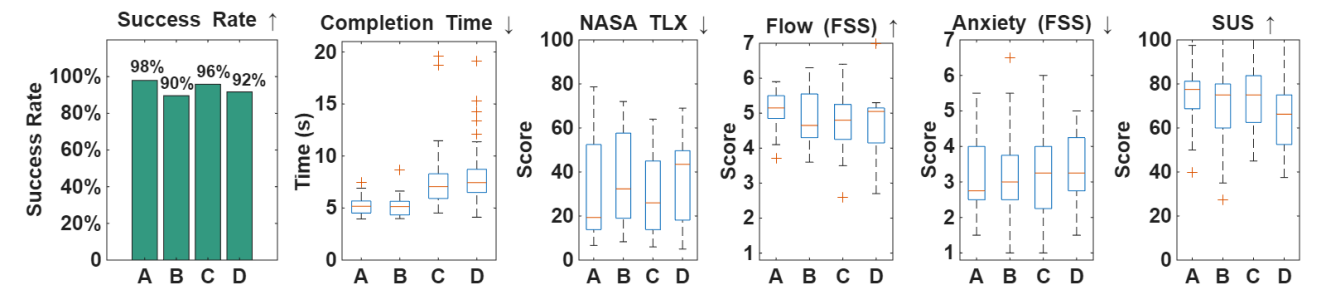


Fig. 5: Summary of results from the user study experiments highlighting the success rate and completion time, as well as scores of the three surveys used for assessment (NASA TLX, FSS, and SUS).

the instructions the first time (e.g., not moving the object at all), they were reminded of the instructions, and a further attempt was made, replacing the previous attempt regardless of its success status.

After each condition, we asked the participants to fill out three surveys: *NASA Task Cognitive Load* (TLX) [31], *Flow Short Scale* (FSS) [32], and *System Usability Scale* (SUS) [33]. At the end of the experiment, each participant was involved in a semi-structured discussion to better understand their preferences and feedback.

C. Experimental Results

We show the success rate, completion time of successful handovers, and survey scores in Fig. 5. Specifically, Condition $\bf A$, which adopted the proposed virtual model control interaction layer and incorporated the proposed augmented reality, led to a high success rate (98%) and the lowest completion time ($M=4.9\mathrm{s}$), which was close to the reported translation approach (see Table II). This indicates the effectiveness of deploying the proposed method for new users

Overall, all four conditions (A–D) delivered high success rates with reasonable completion times. Nonetheless, conditions utilizing augmented reality visuals (A and C) resulted in higher usability and lower task load, with the authoritative robot (A) providing better results than the cooperative robot (C). Moreover, FSS scores indicated inconsistency of augmented reality impact across the two robot profiles. With the authoritative robot, participants were more engaged and experienced lower anxiety levels in the presence of augmented reality visuals, in contrast to the cooperative robot profile, leading to opposite observations.

D. Statistical Analysis

The Shapiro-Wilk test revealed that only completion time under Condition **B** (p=0.0062) and the NASA TLX under Condition **A** (p=0.0098) were not normally distributed. Therefore, we used a non-parametric Friedman test to analyze the mean of the successful trials, which showed a statistically significant difference ($\chi^2=32.4750, df=3, p\leq0.0001$) for the completion time and a non-significant result for NASA TLX ($\chi^2=0.9750, df=3, p=0.8073$).

Post hoc analysis of completion time using the Nemenyi test showed a statistically significant difference between

conditions **A** and **C** (p = 0.0021), conditions **A** and **D** ($p \le 0.0001$), conditions **B** and **C** (p = 0.0035), and conditions **B** and **D** ($p \le 0.0001$). This difference was expected as the cooperative conditions were slower and required a longer time to complete the task.

To analyze the remaining data, we used a one-way repeated measures ANOVA test. The results showed a non-significant difference for the flow (F=0.9699,df=3,p=0.4153), and anxiety (F=0.4620,df=3,p=0.7102) measured using the FSS questionnaire, and the SUS survey scores (F=1.0273,df=3,p=0.3895). These results reflect the slight variation in preferences observed during the semi-structured discussion.

E. Participants' Feedback and Comments

Our semi-structured discussion revealed that 7 participants (43.75%) preferred **A**, 5 (31.25%) preferred **B**, 3 (18.75%) preferred **C**, with only 1 preferring **D**. The 12 participants who preferred the authoritative robot profile mentioned liking the robot's responsiveness and handling most of the task effort. In contrast, those who preferred the cooperative robot liked being involved when giving the object and compensating for any inaccuracies coming from the robot.

Regarding augmented reality visuals, the 10 participants who preferred them mentioned that knowing the expected position of the robot gave them confidence in the task. In contrast, the remaining six participants found the visuals too distracting from the operation of the real robot, aligning with prior findings [28]. Additionally, a handful of participants expressed confusion about when to give the object to the robot with the cooperative robot profile, which hints at a need for better communication of the robot's current state.

VI. CONCLUSION AND FUTURE WORKS

We have proposed a novel approach for human-to-robot object handovers consisting of an interaction layer and augmented reality-based bidirectional communication to enable resilient robotic actions that adapt to dynamic changes during the handover. We utilized virtual model control to implement the interaction layer formed by a set of springs and dampers that interconnect the robotic gripper to a generated target grasping pose around the object held by the human. We demonstrated its resilience by extensively testing it under various sources of variation, including changing the starting

pose of the robot, performing a simple translation or rotation motion of different objects once the robot starts moving, and complex and random variation combinations after the grasping action was initiated.

We also completed a user study that focused on analyzing user preferences regarding the robot's behavior and the augmented reality-based implementation. The study explored the role of augmented reality visual information in connection to resilient-aggressive vs slow-cooperative profiles for the robot behavior. The study showed a strong preference for the resilient robot and a positive response to the augmented reality visuals.

These studies point at the need of an adaptive interaction layer, capable of offering a personalized experience. This will be part of our future research. We also aim to explore further communication cues that will enable humans to understand the current robot state and respond to it promptly with the necessary action.

ACKNOWLEDGMENTS

This work was supported by the Science Research Council and AgriFoRwArdS CDT EP/S023917/1. The Cambridge University Engineering Department Ethics Committee approved the user study and its procedure.

REFERENCES

- H. Duan, Y. Yang, D. Li, and P. Wang, "Human-robot object handover: Recent progress and future direction," *Biomim. Intell. Robot.*, p. 100145, 2024.
- [2] V. Ortenzi, A. Cosgun, T. Pardi, W. P. Chan, E. Croft, and D. Kulić, "Object handovers: a review for robotics," *IEEE Trans. Robot.*, vol. 37, no. 6, pp. 1855–1873, 2021.
- [3] J. Domínguez-Vidal and A. Sanfeliu, "Anticipation and proactivity. unraveling both concepts in human-robot interaction through a handover example," in 2024 33rd IEEE Inter. Conf. on Robot and Human Inter. Comm. (RO-MAN). IEEE, 2024, pp. 957–962.
- [4] D. Liu, X. Wang, M. Cong, Y. Du, Q. Zou, and X. Zhang, "Object transfer point predicting based on human comfort model for humanrobot handover," *IEEE Trans. Instrum. Meas.*, vol. 70, pp. 1–11, 2021.
- [5] W. Wang, R. Li, Y. Chen, Y. Sun, and Y. Jia, "Predicting human intentions in human-robot hand-over tasks through multimodal learning," *IEEE Trans. Autom. Sci. Eng.*, vol. 19, no. 3, pp. 2339–2353, 2021.
- [6] P. Rosenberger, A. Cosgun, R. Newbury, J. Kwan, V. Ortenzi, P. Corke, and M. Grafinger, "Object-independent human-to-robot handovers using real time robotic vision," *IEEE Robot. Autom. Lett.*, vol. 6, no. 1, pp. 17–23, 2020.
- [7] C.-I. Huang, Y.-Y. Huang, J.-X. Liu, Y.-T. Ko, H.-C. Wang, K.-H. Chiang, and L.-F. Yu, "Fed-hanet: Federated visual grasping learning for human robot handovers," *IEEE Robot. Autom. Lett.*, vol. 8, no. 6, pp. 3772–3779, 2023.
- [8] Y. L. Pang, A. Xompero, C. Oh, and A. Cavallaro, "Stereo hand-object reconstruction for human-to-robot handover," *IEEE Robot. Autom. Lett.*, 2025.
- [9] C. Castellani, E. Turco, V. Bo, M. Malvezzi, D. Prattichizzo, G. Costante, and M. Pozzi, "Soft human-robot handover using a vision-based pipeline," *IEEE Robot. Autom. Lett.*, 2024.
- [10] M. Bianchi, G. Averta, E. Battaglia, C. Rosales, M. Bonilla, A. Tondo, M. Poggiani et al., "Touch-based grasp primitives for soft hands: Applications to human-to-robot handover tasks and beyond," in 2018 IEEE Int. Conf. Robot. Autom. (ICRA). IEEE, 2018, pp. 7794–7801.
- [11] W. Yang, C. Paxton, M. Cakmak, and D. Fox, "Human grasp classification for reactive human-to-robot handovers," in 2020 IEEE/RSJ Int. Conf. Intell. Robots Syst. (IROS). IEEE, 2020, pp. 11123–11130.
- [12] W. Yang, C. Paxton, A. Mousavian, Y.-W. Chao, M. Cakmak, and D. Fox, "Reactive human-to-robot handovers of arbitrary objects," in 2021 IEEE Int. Conf. Robot. Autom. (ICRA), pp. 3118–3124.

- [13] G. Zhang, H.-S. Fang, H. Fang, and C. Lu, "Flexible handover with real-time robust dynamic grasp trajectory generation," in 2023 IEEE/RSJ Int. Conf. Intell. Robots Syst. (IROS), pp. 3192–3199.
- [14] H. Duan, P. Wang, Y. Yang, D. Li, W. Wei, Y. Luo, and G. Deng, "Reactive Human-to-Robot Dexterous Handovers for Anthropomorphic Hand," *IEEE Trans. Robot.*, 2024.
- [15] W. Yang, B. Sundaralingam, C. Paxton, I. Akinola, Y.-W. Chao, M. Cakmak, and D. Fox, "Model predictive control for fluid humanto-robot handovers," in 2022IEEE Int. Conf. Robot. Autom. (ICRA). IEEE, 2022, pp. 6956–6962.
- [16] M. Costanzo, G. De Maria, and C. Natale, "Handover control for human-robot and robot-robot collaboration," Front. Robot. AI, vol. 8, p. 672995, 2021.
- [17] M. Djeha, A. Dallard, A. Zermane, P. Gergondet, and A. Kheddar, "Human-robot handovers using task-space quadratic programming," in 2022 31st IEEE Inter. Conf. on Robot and Human Inter. Comm. (RO-MAN), pp. 518–523.
- [18] Z. Wang, J. Chen, Z. Chen, P. Xie, R. Chen, and L. Yi, "Genh2r: Learning generalizable human-to-robot handover via scalable simulation demonstration and imitation," in *IEEE/CVF Comput. Soc. Conf. Comput. Vis. Pattern Recognit.*, 2024, pp. 16362–16372.
- [19] J. E. Pratt, "Virtual model control of a biped walking robot," *Master's thesis*, 1995.
- [20] D. Larby and F. Forni, "Optimal Virtual Model Control for Robotics: Design and Tuning of Passivity-Based Controllers," arXiv:2411, 2024.
- [21] J. Pratt, C.-M. Chew, A. Torres, P. Dilworth, and G. Pratt, "Virtual model control: An intuitive approach for bipedal locomotion," *Int. J. Robot. Res*, vol. 20, no. 2, pp. 129–143, 2001.
- [22] A. Winkler, I. Havoutis, S. Bazeille, J. Ortiz, M. Focchi et al., "Path planning with force-based foothold adaptation and virtual model control for torque controlled quadruped robots," in 2014 IEEE Int. Conf. Robot. Autom. (ICRA), pp. 6476–6482.
- [23] G. Chen, S. Guo, B. Hou, and J. Wang, "Virtual model control for quadruped robots," *IEEE Access*, vol. 8, pp. 140736–140751, 2020.
- [24] Y. Zhang, D. Larby, F. Iida, and F. Forni, "Virtual model control for compliant reaching under uncertainties," in 2024 IEEE/RSJ Int. Conf. Intell. Robots Syst. (IROS). IEEE, 2024, pp. 795–801.
- [25] D. Larby, J. Kershaw, M. Allen, and F. Forni, "Collaborative Drill Alignment in Surgical Robotics," arXiv:2503.05791, 2025.
- [26] R. Suzuki, A. Karim, T. Xia, H. Hedayati, and N. Marquardt, "Augmented reality and robotics: A survey and taxonomy for ar-enhanced human-robot interaction and robotic interfaces," in 2022 ACM Conf. Hum. Factors Comput. Syst., 2022, pp. 1–33.
- [27] S. K. Tadeja, T. Zhou, M. Capponi, K. Walas, T. Bohné, and F. Forni, "Using Augmented Reality in Human-Robot Assembly: A Comparative Study of Eye-Gaze and Hand-Ray Pointing Methods," in 2024 IEEE/RSJ Int. Conf. Intell. Robots Syst. (IROS), 2024, pp. 8786–8793.
- [28] R. Newbury, A. Cosgun, T. Crowley-Davis, W. P. Chan, T. Drummond, and E. A. Croft, "Visualizing robot intent for object handovers with augmented reality," in 2022 31st IEEE Inter. Conf. on Robot and Human Inter. Comm. (RO-MAN). IEEE, 2022, pp. 1264–1270.
- [29] D. Larby, "VMRobotControl.jl," https://github.com/Cambridge-Control-Lab/VMRobotControl, 2024.
- [30] G. d. M. Costa, M. R. Petry, and A. P. Moreira, "Augmented reality for human–robot collaboration and cooperation in industrial applications: A systematic literature review," *Sensors*, vol. 22, no. 7, p. 2725, 2022.
- [31] S. Hart and L. Staveland, "Development of NASA-TLX (Task Load Index): Results of Empirical and Theoretical Research," Advances in Psychology, pp. 139–183, 1988.
- [32] S. Engeser and F. Rheinberg, "Flow, performance and moderators of challenge-skill balance," *Motiv. Emot.*, vol. 32, no. 3, pp. 158–172, Sep. 2008.
- [33] J. Brooke, "SUS: A 'Quick and Dirty' Usability Scale," vol. 189, pp. 189–194, November 1996.